

## Original Article

# On the Path to High-temperature Josephson Multi-junction Devices

Xu Wang<sup>1</sup>, Fucong Chen<sup>1</sup>, Zefeng Lin<sup>1</sup>, Changhong Yuan<sup>1</sup>, Shibing Tian<sup>1</sup>, Chunguang Li<sup>1</sup>, Victor Kornev<sup>2</sup>, and Nikolay Kolotinskiy<sup>2</sup>

1. *Institute of Physics, Chinese Academy of Sciences, Beijing, China*

2. *Faculty of Physics, Lomonosov Moscow State University, Moscow, Russia*

Corresponding author: Xu Wang; Email: risingsunwx@iphy.ac.cn.

Received March 11, 2024; Accepted August 30, 2024.

This work was supported by National Key R&D Program of China 2022YFA1603900 and in part by Russian Science Foundation (RSCF) grant no. 19-72-10016-P.

Copyright © 2024 The Authors. This is a gold open access article under a Creative Commons Attribution License (CC BY 4.0).

**Abstract** — We report our progress in the high-temperature superconductor (HTS) Josephson junction fabrication process founded on using a focused helium ion beam damaging technique and discuss the expected device performance attainable with the HTS multi-junction device technology. Both the achievable high value of characteristic voltage  $V_c = I_c R_N$  of Josephson junctions and the ability to design a large number of arbitrary located Josephson junctions allow narrowing the existing gap in design abilities for LTS and HTS circuits even with using a single YBCO film layer. A one-layer topology of active electrically small antenna is suggested and its voltage response characteristics are considered.

**Keywords** — Josephson junctions, high-temperature superconductors, YBCO, focused helium ion beam fabrication technique, Josephson multi-junction devices, SQUID, active electrically small antenna

## I. Introduction

Superconductive electronics technologies leverage the distinctive macroscopic quantum phenomena exhibited by superconductors. These phenomena include superconductivity, magnetic flux quantization, and the effect of macroscopic quantum interference and Josephson effect [1–3], which are applicable across a wide range of frequencies from direct current (dc) to very high frequencies. In fact, degradation of the Josephson junction properties relevant to their applications starts only at Josephson oscillation frequencies exceeding the characteristic Josephson junction frequency

$$F_c = V_c / \Phi_0 = I_c R_N / \Phi_0, \quad (1)$$

where  $V_c$ ,  $I_c$  and  $R_N$  are the junction characteristic voltage, critical current, and resistance in the normal state, respectively, and  $\Phi_0 = h/2e$  represents the flux quantum.  $F_c$  can reach hundreds of gigahertz and beyond. In addition, losses in superconductors remain low until reaching the gap frequency [3] (for example, the gap frequency of Nb is about 700 GHz). All these properties enable the development of a variety of superconductor devices and circuits [1, 3] with characteristics unattainable for semiconductor electronic technology. Among those, there is diverse range of digital

and mixed-signal superconductive circuits, namely analog-to-digital converters (ADC) [4–8] and integrated digital circuits [9], including prototypes of microprocessors [10–12], which can operate at frequencies with tens of gigahertz and even higher [13]. These devices are powered by the Rapid Single Flux Quantum (RSFQ) logic [14–22], which operates using single flux quanta of magnetic flux  $\Phi_0 = h/2e$  for data signals and clock. In the RSFQ circuits, a single switching event of an overdamped Josephson junction (at  $R_N C < 1/(2\pi F_c)$ , where  $C$  is the capacitance of a junction [4]) with a typical  $I_c \sim 100 \mu\text{A}$  dissipates an extremely low energy of  $E_J = \Phi_0 I_c \sim 10^{-19} \text{ J}$ . Moreover, the switching time  $\tau$  of the junction is about  $10^{-12} \text{ s}$ , allowing for clock frequencies in the hundreds of gigahertz range (*e.g.* see [13]).

Multiple Josephson junction devices can essentially improve the sensitivity and bandwidth of superconducting analog devices. Among them are SQUID-based array amplifiers [23], traveling wave parametric amplifiers [24–27], as well as Superconducting Quantum Filters (SQIFs) [28, 29] and Superconducting Quantum Arrays (SQAs) [30] allowing implementation of highly sensitive active electrically small antennas (ESAs) capable of providing both the reception and amplification of an incident electromagnetic wave [31, 32].

Such broadband ESAs can improve overall performance of superconductive broadband digital-rf receivers based on direct signal digitization allowing then digital extraction of customizable sub-bands [33, 34]. As reported in [35–37], the receivable signal frequency can be ranged from VHF to K frequency bands.

These advances in the superconductive electronics have been achieved mainly by the use of low-temperature superconductors (LTS) and first of all a niobium fabrication process based on using tunnel Josephson junctions [3] with aluminum oxide barrier (*e.g.* see [38]). The implementation of high-temperature superconductor (HTS) devices, other than the simplest ones containing only a few Josephson junctions, poses a stiff challenge because of substantial design restrictions within the grain-boundary junction fabrication techniques (with either bi-crystal or step-edge or ramp-edge junctions) [3] which have been generally used until now. In spite of that, much simpler array-type HTS structures but composed of great deal of Josephson junctions were nevertheless realized using fabrication technique of step-edge Josephson junctions [39]. Such a SQIF-like 2D network containing in whole 54000 SQUIDS showed a magnetic field to voltage transfer function with a central peak value of approximately 8 mV and a highly linear central peak portion around 4.5 mV [39].

Because of the short coherence length and small capacitance, ideal HTS SIS junction with hysteresis is very difficult to realize. Most HTS junctions exhibited a current-voltage (IV) curve similar to that of the LTS weak-link junctions. Various types HTS Josephson junctions such as bicrystal, step-edge, ramp-edge and ion-beam damaged junctions have been realized and compared in reviews and books [3]. Among these techniques, the ion-beam damaging technique can obtain a controllable local suppression of superconducting properties of HTS films down to metallic or even to dielectric properties. When a focused ion beam is used, it enables forming a narrow barrier across a superconducting strip to realize a weak link between the strip parts and hence a Josephson junction with characteristics depending on irradiation dose [40, 41]. Such a technique provides basis for a highly promising fabrication process enabling creation of high-quality multi-junction HTS devices. In fact, one can refer to [42–44] where the ion-beam damaging impact on HTS films of  $\text{YBa}_2\text{Cu}_3\text{O}_{7-x}$  (YBCO) has been already used to fabricate series SQIFs consisting of 300 to 2000 dc SQUIDS. Being in an unshielded magnetic environment, these devices were able to measure magnetic signals as low as a few pT in a frequency band ranged up to 1.125 GHz. Besides, the devices showed a linear voltage response over 7 decades in RF power, that is a highly encouraging achievement.

In this paper, we report our progress in the HTS Josephson junction fabrication process founded on using a focused helium ion beam damaging effect and discuss the expected

device performance attainable for the HTS multi-junction device technology.

## II. Progress in HTS Josephson junction fabrication

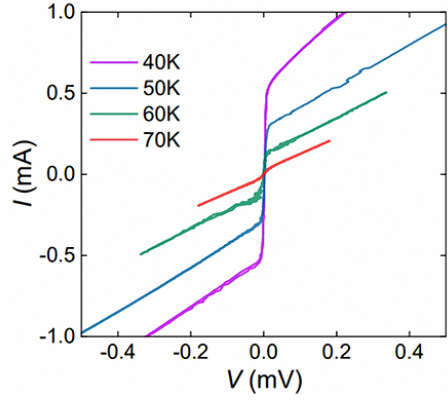
The localized impact of the helium ion irradiation on a  $\text{YBa}_2\text{Cu}_3\text{O}_{7-x}$  (YBCO) HTS film can provide a local damage of the film structure resulting in local degradation of the film superconducting properties with irradiation dose down to normal metal conductivity and then to dielectric behavior [40]. By using the focused helium ion beam, the damaged film area across a film strip can be made very narrow to provide weak electric coupling between the strip parts of metallic or tunnelling types that enables forming Josephson junctions which can have properties of SNS to SIS type junctions [45].

We used YBCO films deposited on STO substrates by pulsed laser deposition (PLD) technique. The films deposited at high oxygen pressure are grown epitaxially together with the substrate and therefore are highly crystalline with a highly uniform crystal orientation. Furthermore, the films deposited at high oxygen pressure also demonstrate a reasonably low microwave surface resistance of about 0.7 m $\Omega$  per square (77 K, 9.4 GHz) [46].

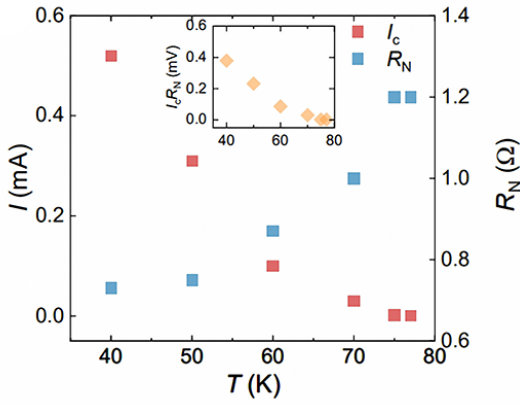
To fabricate and study the focused helium ion beam Josephson junctions, 4  $\mu\text{m}$ -wide film bridges (with 4 electrodes to enable four-point measurement of IV curve) were patterned with electron beam lithography (EBL) on a 35 nm thick YBCO thin film with an *in situ* deposited Au layer on the top. For the EBL process, the acceleration voltage of electrons was 10 keV and the beam current was about 0.2 nA. The Au layer on the bridges was removed by wet etching. Next, a 35 kV helium beam was used to write on the bridges by crossing the 4-micrometer-wide superconducting film bridges, thereby forming narrow damaged areas and hence to form Josephson junctions with irradiation dose changing from 100 ions/nm to 700 ions/nm. Resistance of the damaged area as a barrier between the film strip parts shows the temperature dependence corresponding to the metal type barrier at a lower dose and gradually varying to the insulator like barrier with the dose increase.

Figure 1 shows IV curves (a), critical current  $I_c$ , normal resistance  $R_N$ , and their product (characteristic voltage)  $I_c R_N$  (b) of the Josephson junctions written with an irradiation dose of 200 ions/nm, which are measured at different temperatures of 40, 50, 60 and 70 K. At 40 K, the critical current value is about 0.5 mA, which corresponds to a critical current density  $3.6 \times 10^5 \text{ A/cm}^2$  according to the bridge width and film thickness, while the normal resistance is about 0.8  $\Omega$ , that results in the characteristic voltage value  $V_c \simeq 0.4 \text{ mV}$ . As shown in Fig. 1b, the normal resistance decreases with temperature decreasing and hence manifests a normal metal type of the junction barrier.

Figure 2 shows IV curves (a), critical current  $I_c$ , normal resistance  $R_N$ , and their product (characteristic voltage)

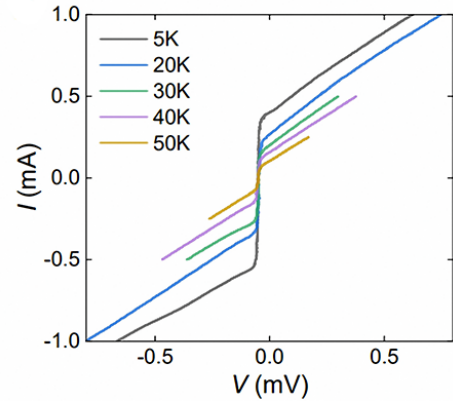


(a)

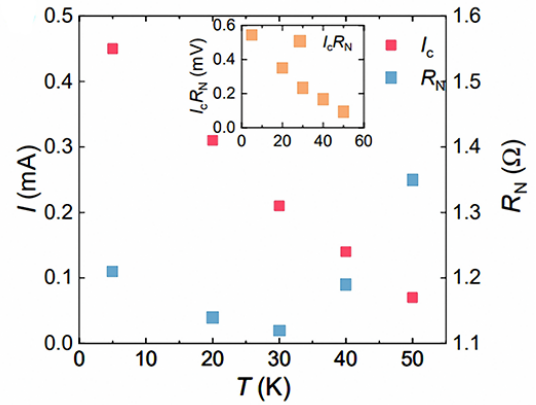


(b)

**Figure 1** IV curves (a), critical current  $I_c$ , normal resistance  $R_N$  (b), and their product (characteristic voltage)  $I_c R_N$  (inset) of the Josephson junctions fabricated using a helium dose of 200 ions/nm, which are measured at different temperatures: 40, 50, 60 and 70 K.



(a)



(b)

**Figure 2** IV curves (a), critical current  $I_c$ , normal resistance  $R_N$  (b), and their product (characteristic voltage)  $I_c R_N$  (inset) of the Josephson junctions fabricated using a helium dose of 300 ions/nm, which are measured at different temperatures: 5, 20, 30, 40 and 50 K.

$I_c R_N$  (b) of the Josephson junctions written with a dose of 300 ions/nm, which are measured at different temperatures from 5 K to 50 K. At 40 K, the critical current value is about 0.14 mA, which corresponds to a critical current density  $1 \times 10^5$  A/cm<sup>2</sup>, while the normal resistance is about 1.19 Ω, that results in the characteristic voltage value  $V_c \simeq 0.16$  mV. For this junction, the normal resistance first decreases but then increases with temperature decreasing, indicating a barrier property somehow between metal and insulator.

Further increasing the helium dose, Fig. 3 shows IV curves (a), critical current  $I_c$ , normal resistance  $R_N$ , and their product (characteristic voltage)  $I_c R_N$  (b) of the Josephson junctions fabricated using a dose of 400 ions/nm, which are measured at different temperatures from 5 to 40 K. At 40 K, the critical current value is about 60 μA, which corresponds to a critical current density  $4.3 \times 10^4$  A/cm<sup>2</sup>, while the normal resistance is about 2 Ω, that results in the characteristic voltage value  $V_c \simeq 0.12$  mV. For the junction written with a dose

of 400 ions/nm, the normal resistance increases with temperature decreasing in contrast to the junctions written with a dose of 200 ions/nm. This fact indicates rather insulator-close type of the junction barrier. Hence, by simply controlling the helium dose parameter, the barrier characteristic can be regulated gradually, which benefits the following multi-junction device designing.

As one can see from Figs. 1 to 3, the fabricated HTS Josephson junctions show IV curves closed to the ones corresponding to the resistively shunted junction model (RSJ model) [2] of overdamped Josephson junctions (when the capacitive parameter, usually called as Stewart-McCumber parameter,

$$\beta_c = (2e/\hbar) I_c R_N^2 C \ll 1, \quad (2)$$

where  $C$  is the junction capacitance) [2]. This is just the type of the junctions which are needed for designing a major part of the promising superconductor devices. Moreover, the obtained characteristic voltage values  $V_c \simeq (0.12 \text{ to } 0.4)$  mV at

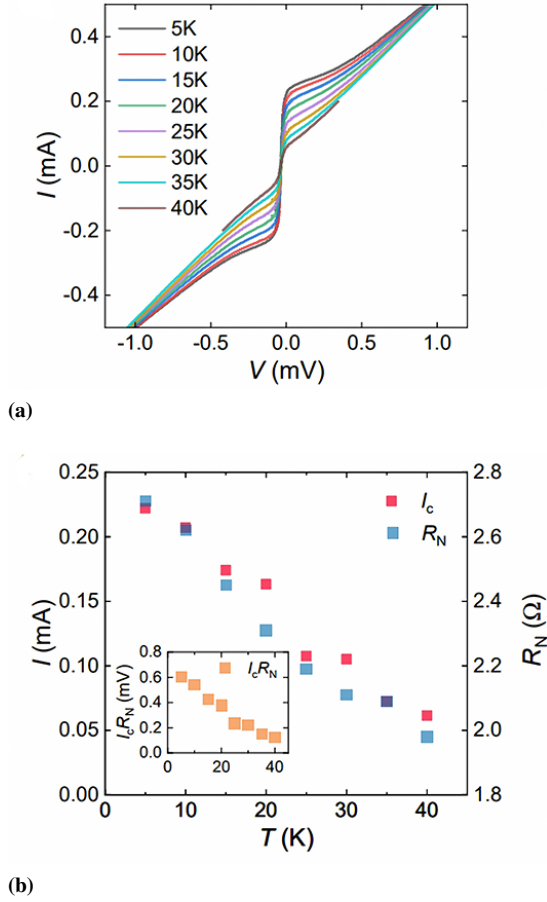


**Figure 3** IV curves (a), critical current  $I_c$ , normal resistance  $R_N$  (b), and their product (characteristic voltage)  $I_c R_N$  (inset) of the Josephson junctions fabricated using a helium dose of 400 ions/nm, which are measured at different temperatures: 5 to 40 K.

40 K are quite high and comparable with the ones of the resistively shunted Nb tunnel junctions. In fact, at the often-used critical current density  $j_c = 4.5 \text{ kA/cm}^2$  and  $I_c \simeq 0.1 \text{ mA}$ , requirement (2) yields in  $V_C \lesssim 0.4 \text{ mV}$  (see design parameters in [38]). Besides, the reported values of  $V_C$  are not so much less than the best ones feasible for the grain-boundary junctions: 1 to 3 mV at temperature 4.2 K and 0.1 to 0.3 mV at 77 K as summarized in [3, p. 323]. One can expect more progress in the Josephson junction parameters with further refinement of the fabrication technology.

### III. Discussion

Main advantages of the focused helium ion beam fabrication technique developed and reported here are: (i) the achievable high value of the characteristic voltage  $V_C = I_c R_N$  of the YBCO Josephson junctions; (ii) the controllable barrier characteristic; (iii) the ability to design a large number of arbitrary located Josephson junctions. These facts allow narrowing the existing gap in design abilities for LTS and HTS circuits even

with using only single HTS film layer.

Characteristic voltage  $V_C$  of Josephson junctions is important figure of merit for device application. The increase in  $V_C$  of the used Josephson junctions essentially improves performance of all Josephson junction devices, including single dc SQUIDs and more complicated SQUID-based devices, by increase (i) in the output voltage and the flux-to-voltage transfer factor, both are proportional to  $V_C$ , and hence in dynamic range of the devices [32], (ii) in the maximum signal (averaged over Josephson oscillations) frequency  $F_{\text{sign}} \ll F_C$  through increase in the characteristic Josephson-junction frequency  $F_C$  (1).

One of such simple and highly promising devices which can be realized using the single-layer topology is active broadband receiving electrically small antenna (ESA) based on using differential dc SQUID circuit (DSQUID) [47]. Figure 4 shows a schematic layout of the active ESA which can be formed on chip of very small size  $a \times a$  such as 5 by 5 mm<sup>2</sup> or even less and therefore can be capable of receiving electromagnetic signals through sensing their magnetic component  $B$  in the wide frequency band starting from dc.

The antenna contains quadratic superconducting strip loop and two dc SQUIDs inside the loop. The SQUIDs are biased independently by means of two current sources, each

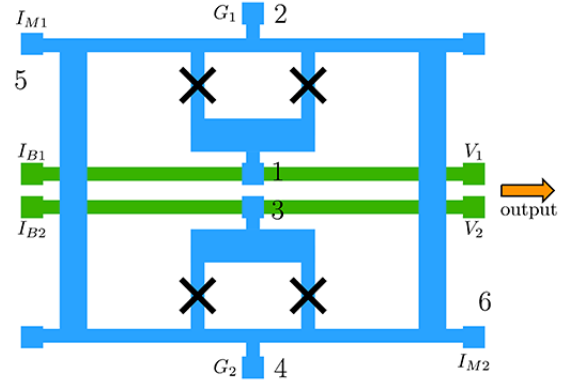


**Figure 4** Schematic layout of the one-layer active ESA based on using DSQUID [47]. Superconductor film strips are shown by blue color, while normal metal lines (wires for connection) are shown by green color. The antenna contains quadratic superconducting strip loop and two dc SQUIDs inside the loop. The SQUIDs are biased independently by means of two current sources, each applying dc bias current  $I_b \simeq 2I_c$  are connected to points 1, 2 and 3, 4, respectively. The points 2 ( $G_1$ ) and 4 ( $G_2$ ) are to be connected via some resistors to a normal metal ground (this connection is not shown). Output signal is voltage  $V$  measured between points 1, 3. An incident electromagnetic wave (namely, a flux of its magnetic field component) induces circular screening current in the superconducting loop. This current applies magnetic flux to both dc SQUIDs. An additional source of dc current  $I_m$  is connected to points 5,6 to apply dc magnetic flux  $\Phi_m \lesssim \Phi_0/4$  to each of the dc SQUIDs but with opposite signs. The antenna output voltage  $V = V_1 - V_2$  is measured between points 1,3.



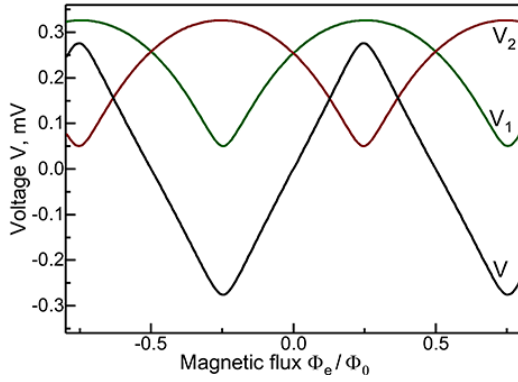


**Figure 5** Voltage responses  $V_1$ ,  $V_2$  of both dc SQUIDs with  $l = 2$  and resulting voltage response  $V = V_1 - V_2$  of the antenna at  $I_b = 2I_c$  obtained by means of numerical simulation using PSCAN software [48, 49]. Here  $\Phi_e$  is the magnetic flux applied to each of dc SQUIDs;  $\Phi_e = \Phi_{ex}M/L_{ant}$ , where  $\Phi_{ex}$  is the flux applied to the antenna loop area by an incident electromagnetic wave,  $L_{ant}$  is the antenna loop inductance, and  $M$  is the mutual inductance between the antenna loop and dc SQUID loop. Voltage scale is given for the case of using YBCO Josephson junctions with characteristic voltage  $V_c = 0.4$  mV).

applying dc bias current  $I_b = 2I_c$ , connected to points 1, 2 and 3, 4, respectively. The points 2 (G1) and 4 (G2) are to be connected via some resistors to a normal metal ground (this connection is not shown in Fig. 4). Output signal is voltage  $V = V_1 - V_2$  measured between points 1, 3.

A circular screening current is induced by an incident electromagnetic wave (namely, by a flux of its magnetic field component) in the superconducting loop, and therefore applies magnetic flux  $\Phi_e$  to each of the dc SQUIDs. An additional source of dc current  $I_m$  is connected to points 5, 6 to apply dc magnetic flux  $\Phi_m \lesssim \Phi_0/4$  to each of the dc SQUIDs but with opposite signs to shift voltage responses of the dc SQUIDs in opposite directions.

Figure 5 shows the voltage responses  $V_1$ ,  $V_2$  of both dc SQUIDs (measured between points 1, 2 and 3, 4, respectively) and resulting voltage response of the antenna  $V = V_1 - V_2$  versus magnetic flux  $\Phi_e$  applied to each of the two dc SQUIDs. The responses were obtained by numerical simulation using PSCAN software [48, 49]. As far as form of the voltage response of dc SQUID at the critical current biasing  $I_b = 2I_c$  is very close to parabolic law, the difference of the mutually shifted voltage responses (by dc flux  $\Phi_m$ ) voltage responses ( $V_1$  and  $V_2$ ), which is the antenna voltage measured between points 1, 3, shows linear response to the incident wave. The linear response range allows the peak-to-peak value of the signal magnetic flux  $\Phi_e$  up to about  $\Phi_0/2$ .

When normalized inductance of the used dc SQUIDs

$$l = \frac{2\pi I_c L}{\Phi_0} \quad (3)$$

is much less than 1, maximum swing of the antenna voltage

response  $\Delta V$  can be at  $I_b = 2I_c$  as high as  $2V_c$  resulting in the flux-to-voltage transfer factor value

$$V_\Phi = dV/d\Phi_{ex} = 4V_c/\Phi_0 \quad (4)$$

Both  $\Delta V$  and  $V_\Phi$  decrease with increase in the bias current  $I_b$  and with increase in normalized inductance  $l$  [2, 3].

Sensitivity of the antenna to the flux  $\Phi_e$  applied to each of the dc SQUIDs (internal sensitivity) is given by ratio of the *rms* value  $V_f$  of the output voltage noise to the transfer factor  $V_\Phi$ . In compliance with Langevin method, the noise current component through Josephson junction (JJ) generated by its  $R_N$  can be described through parallel connection of noiseless JJ and noise current source with the proper spectrum density  $S_I$ , which in the thermal noise limit is  $S_I = 4k_B T/R_N$ , where  $k_B$  is the Boltzmann's constant and  $T$  is the ambient temperature. In view of independence of the noise sources, the *rms* value  $V_f$  can be estimated, using approximation of the effective differential resistance of JJ in resistive state by  $R_N$ , as follows:

$$V_f \simeq \{2[2S_I R_N^2/4]\Delta F\}^{1/2} = 2\sqrt{k_B T R_N \Delta F}, \quad (5)$$

where  $\Delta F$  is the frequency band of the subsequent registering unit. Thus, the internal sensitivity is as follows:

$$\Delta\Phi_e/\sqrt{\Delta F} = V_f/V_\Phi \approx \Phi_0 \sqrt{k_B T R_N}/(2V_c). \quad (6)$$

This characteristic improves with characteristic voltage  $V_c$  of the used Josephson junctions.

At a fixed size of dc SQUID loops and hence their inductance  $L$ , resulting sensitivity of the active ESA to the incident electromagnetic wave rises proportionally to the linear size  $a$  of the antenna loop, while the antenna remains electrically small (at  $a \lesssim \lambda/6$ ). In fact, the signal magnetic flux  $\Phi_e$  applied by the incident wave to each of the dc SQUID  $s$  is proportional to the screening current induced in the antenna loop  $I_{ant} = BS_{ant}/L_{ant}$ , where  $B$  is the magnetic field component perpendicular to the antenna chip plane,  $S_{ant}$  is the antenna loop area, and  $L_{ant}$  is the antenna loop inductance. This current and hence  $\Phi_e$  both rise proportionally to the antenna size  $a$  since  $S_{ant}$  is proportional to  $a^2$ , while  $L_{ant}$  is proportional to  $a$ .

When  $a \gtrsim \lambda/6$ , one has to take into consideration an appeared inhomogeneity in the magnetic field distribution along the antenna length. In case of a harmonic incident wave, such a consideration results in decrease of the applied magnetic flux amplitude described by factor

$$D = \sin(\pi a/\lambda)/(\pi a/\lambda). \quad (7)$$

This factor gives a 3 dB reduction in the flux amplitude and hence in amplitude of the antenna output voltage at  $\lambda_0 \simeq 9a/4 = 2.25a$ . Thus, the value  $\lambda_0$  sets the upper frequency of the antenna band starting from dc

Further development of the active electrically small antenna (ESA) can be obtained by replacing two dc SQUIDs by two parallel arrays of Josephson junctions, i.e. with realizing a particular case of active ESA based on SQA (superconducting quantum array) [30] composed of differential unit blocks [32]. Such a design approach can be used also to develop high-performance rf amplifiers.

The use of multi-junction array structures like SQAs [30] or SQIF [28, 29] enables an increase of overall device performance, including increase in dynamic range of the multi-junction devices, through increase in signal-to-noise ratio (SNR) with the number  $N$  of unit cells proportional to  $\sqrt{N}$ . In fact, as long as intrinsic fluctuations in array cells are independent, spectral density of the low-frequency voltage fluctuations (at the signal frequency  $\Omega$ ) across the serially connected  $N$  cells  $S_V(\Omega) = NS_V^0(\Omega)$ , where  $S_V^0(\Omega)$  is the spectral density across one cell. Thus, the *rms* fluctuation voltage  $V_F = \sqrt{NS_V^0(\Omega)\Delta\Omega}$ , where  $\Delta\Omega$  is the frequency band, increases as  $\sqrt{N}$ , whereas both the maximum output signal  $V_{\max}$  and transfer factor  $V_\Phi = dV/d\Phi$  of the flux  $\Phi$  to voltage  $V$  transformation increases as  $N$ . Therefore, dynamic range  $DR = V_{\max}/V_F$  increases as  $\sqrt{N}$ . In case of  $N$  cells connected in parallel, both the maximum output voltage  $V_{\max}$  and transfer factor  $V_\Phi$  don't change with  $N$ , while the spectral density of the low frequency current fluctuations becomes  $N$  times higher than the one for one cell  $S_I^0(\Omega)$ , and therefore the *rms* fluctuation voltage  $V_F = R_d^0 \sqrt{NS_I^0(\Omega)\Delta\Omega}/N$ , where  $R_d^0 = dV/dI$  is differential resistance at operation point on IV curve of one cell, decreases as  $1/\sqrt{N}$ , and hence dynamic range  $DR = V_{\max}/V_F$  increases also as  $\sqrt{N}$ .

#### IV. Conclusion

The obtained progress in the HTS (YBCO) Josephson junction fabrication process founded on using a focused helium ion beam damaging technique enables achieving characteristic voltage value  $V_c = I_c R_N$  up to about 0.4 mV and potentially higher. Both the high value of  $V_c$  of Josephson junctions and the ability to design a large number of arbitrary located Josephson junctions allow narrowing the existing gap in design abilities for LTS and HTS circuits even with using a single HTS film layer. A one-layer topology of active electrically small antenna is suggested and the antenna voltage response characteristics are considered. Such a design approach can be also used to develop high-performance rf amplifiers. Further development of the active devices can be obtained by using multi-junction array structures like SQAs which enables an increase in overall performance, including increase in dynamic range of the multi-junction devices, through increase of signal-to-noise ratio (SNR) with the number  $N$  of unit cells proportional to  $\sqrt{N}$ .

#### References

- [1] D. A. Cardwell, D. C. Larbalestier, and A. I. Braginski, *Handbook of Superconductivity: Characterization and Applications*, CRC Press, ISBN 9781003139638, doi:10.1201/9781003139638, 2022.
- [2] K. Likharev, *Dynamics of Josephson Junctions and Circuits*, Gordon and Breach Science Publishers, ISBN 9782881240423, 1986.
- [3] P. Seidel (Ed.), *Applied Superconductivity*, Wiley-VCH Verlag GmbH & Co. KGaA, Encyclopedia of Applied Physics, ISBN 978-3-527412-09-9, doi:10.1002/9783527670635, 2015.
- [4] O. Mukhanov, D. Gupta, A. Kadin, and V. Semenov, "Superconductor analog-to-digital converters", *Proceedings of the IEEE*, vol.92, no.10, pp.1564–1584, doi:10.1109/jproc.2004.833660, 2004.
- [5] A. Inamdar, S. Rylov, A. Talalaevskii, A. Sahu, *et al.*, "Progress in design of improved high dynamic range analog-to-digital converters", *IEEE Transactions on Applied Superconductivity*, vol.19, no.3, pp.670–675, doi:10.1109/tasc.2009.2017767, 2009.
- [6] I. Vernik, D. Kirichenko, T. Filippov, A. Talalaevskii, *et al.*, "Superconducting high-resolution low-pass analog-to-digital converters", *IEEE Transactions on Applied Superconductivity*, vol.17, no.2, pp.442–445, doi:10.1109/tasc.2007.898613, 2007.
- [7] S. Sarwana, D. Kirichenko, D. Gupta, and A. Kirichenko, "Dual-band ADC utilizing switch matrix", *IEEE Transactions on Applied Superconductivity*, vol.19, no.3, pp.661–664, doi:10.1109/tasc.2009.2018533, 2009.
- [8] D. Gupta, A. Inamdar, D. E. Kirichenko, A. M. Kadin, and O. A. Mukhanov, "Superconductor analog-to-digital converters and their applications", in *Microwave Symposium Digest (MTT), 2011 IEEE MTT-S International*, IEEE, pp.1–4, doi:10.1109/mwsysym.2011.5973407, 2011, ISSN 0149-645X.
- [9] Q. P. Herr, J. Osborne, M. J. A. Stoutimore, H. Hearne, *et al.*, "Reproducible operating margins on a 72 800-device digital superconducting chip", *Superconductor Science and Technology*, vol.28, no.12, article no.124003, doi:10.1088/0953-2048/28/12/124003, 2015.
- [10] Y. Yamanashi, M. Tanaka, A. Akimoto, H. Park, *et al.*, "Design and implementation of a pipelined bit-serial sfq microprocessor, core1 $\beta$ ", *IEEE Transactions on Applied Superconductivity*, vol.17, no.2, pp.474–477, doi:10.1109/tasc.2007.898606, 2007.
- [11] T. V. Filippov, A. Sahu, A. F. Kirichenko, I. V. Vernik, *et al.*, "20ghz operation of an asynchronous wave-pipelined rsfq arithmetic-logic unit", *Physics Procedia*, vol.36, pp.59–65, doi:10.1016/j.phpro.2012.06.130, 2012.
- [12] Y. Ando, R. Sato, M. Tanaka, K. Takagi, *et al.*, "Design and demonstration of an 8-bit bit-serial RSFQ microprocessor: CORE e4", *IEEE Transactions on Applied Superconductivity*, vol.26, no.5, pp.1–5, doi:10.1109/tasc.2016.2565609, 2016.
- [13] T. V. Filippov, A. Sahu, D. E. Kirichenko, M. E. Çelik, and D. Gupta, "Experimental evaluation of josephson balanced comparators toward 100 GHz RSFQ circuits", *IEEE Transactions on Applied Superconductivity*, vol.34, no.3, pp.1–5, doi:10.1109/tasc.2024.3351626, 2024.
- [14] O. Mukhanov, V. Semenov, and K. Likharev, "Ultimate performance of the RSFQ logic circuits", *IEEE Transactions on Magnetics*, vol.23, no.2, pp.759–762, doi:10.1109/tmag.1987.1064951, 1987.
- [15] S. Polonsky, V. Semenov, P. Bunyk, A. Kirichenko, *et al.*, "New RSFQ circuits (josephson junction digital devices)", *IEEE Transactions on Applied Superconductivity*, vol.3, no.1, pp.2566–2577, doi:10.1109/77.233530, 1993.
- [16] P. Bunyk, K. Likharev, and D. Zinoviev, "RSFQ technology: Physics and devices", *International Journal of High Speed Electronics and Systems*, vol.11, no.01, pp.257–305, doi:10.1142/s012915640100085x, 2001.
- [17] O. A. Mukhanov, "Energy-efficient single flux quantum technology", *IEEE Transactions on Applied Superconductivity*, vol.21, no.3,

- pp.760–769, doi:10.1109/tasc.2010.2096792, 2011.
- [18] D. E. Kirichenko, S. Sarwana, and A. F. Kirichenko, “Zero static power dissipation biasing of rsfq circuits”, *IEEE Transactions on Applied Superconductivity*, vol.21, no.3, pp.776–779, doi:10.1109/tasc.2010.2098432, 2011.
  - [19] M. H. Volkmann, A. Sahu, C. J. Fourie, and O. A. Mukhanov, “Implementation of energy efficient single flux quantum digital circuits with sub-aj/bit operation”, *Superconductor Science and Technology*, vol.26, no.1, article no.015002, doi:10.1088/0953-2048/26/1/015002, 2012.
  - [20] Q. P. Herr, A. Y. Herr, O. T. Oberg, and A. G. Ioannidis, “Ultra-low-power superconductor logic”, *Journal of Applied Physics*, vol.109, no.10, article no.103903, doi:10.1063/1.3585849, 2011.
  - [21] N. Takeuchi, D. Ozawa, Y. Yamanashi, and N. Yoshikawa, “An adiabatic quantum flux parametron as an ultra-low-power logic device”, *Superconductor Science and Technology*, vol.26, no.3, article no.035010, doi:10.1088/0953-2048/26/3/035010, 2013.
  - [22] D. S. Holmes, A. L. Ripple, and M. A. Manheimer, “Energy-efficient superconducting computing – power budgets and requirements”, *IEEE Transactions on Applied Superconductivity*, vol.23, no.3, pp.1701610–1701610, doi:10.1109/tasc.2013.2244634, 2013.
  - [23] M. E. Huber, P. A. Neil, R. G. Benson, D. A. Burns, *et al.*, “Dc squid series array amplifiers with 120 mhz bandwidth”, *IEEE Transactions on Applied Superconductivity*, vol.11, no.2, pp.4048–4053, doi:10.1109/77.947383, 2001.
  - [24] C. Macklin, K. O’Brien, D. Hover, M. E. Schwartz, *et al.*, “A near-quantum-limited josephson traveling-wave parametric amplifier”, *Science*, vol.350, no.6258, pp.307–310, doi:10.1126/science.aaa8525, 2015.
  - [25] T. C. White, J. Y. Mutus, I.-C. Hoi, R. Barends, *et al.*, “Traveling wave parametric amplifier with josephson junctions using minimal resonator phase matching”, *Applied Physics Letters*, vol.106, no.24, article no.242601, doi:10.1063/1.4922348, 2015.
  - [26] M. Bell and A. Samolov, “Traveling-wave parametric amplifier based on a chain of coupled asymmetric SQUIDS”, *Physical Review Applied*, vol.4, no.2, article no.024014, doi:10.1103/physrevapplied.4.024014, 2015.
  - [27] A. Zorin, “Josephson traveling-wave parametric amplifier with three-wave mixing”, *Physical Review Applied*, vol.6, no.3, article no.034006, doi:10.1103/physrevapplied.6.034006, 2016.
  - [28] P. Caputo, J. Tomes, J. Oppenlander, C. Haussler, *et al.*, “Superconducting quantum interference filters as absolute magnetic field sensors”, *IEEE Transactions on Applied Superconductivity*, vol.15, no.2, pp.1044–1047, doi:10.1109/tasc.2003.850193, 2005.
  - [29] J. Oppenländer, T. Träuble, C. Häussler, and N. Schopohl, “Superconducting multiple loop quantum interferometers”, *IEEE Transactions on Applied Superconductivity*, vol.11, no.1, pp.1271–1274, doi:10.1109/77.919581, 2001.
  - [30] V. K. Kornev, A. V. Sharafiev, I. I. Soloviev, N. V. Kolotinskiy, *et al.*, “Superconducting quantum arrays”, *IEEE Transactions on Applied Superconductivity*, vol.24, no.4, pp.1–6, doi:10.1109/tasc.2014.2318291, 2014.
  - [31] V. K. Kornev, A. V. Sharafiev, I. I. Soloviev, N. V. Kolotinskiy, and O. A. Mukhanov, “A guide to active antennas based on superconducting quantum arrays”, *IEEE Transactions on Applied Superconductivity*, vol.26, no.3, pp.1–4, doi:10.1109/tasc.2016.2524461, 2016.
  - [32] V. K. Kornev, N. V. Kolotinskiy, A. V. Sharafiev, I. I. Soloviev, and O. A. Mukhanov, “Broadband active electrically small superconductor antennas”, *Superconductor Science and Technology*, vol.30, no.10, article no.103001, doi:10.1088/1361-6668/aa7a52, 2017.
  - [33] D. Brock, O. Mukhanov, and J. Rosa, “Superconductor digital RF development for software radio”, *IEEE Communications Magazine*, vol.39, no.2, pp.174–179, doi:10.1109/35.900649, 2001.
  - [34] D. Gupta, O. Mukhanov, A. Kadin, J. Rosa, and D. Nicholson, “Benefits of superconductor digital-rf transceiver technology to future wireless systems”, in *Proc. SDR Technical Conference*, vol.1, pp.221–226, 2002.
  - [35] I. V. Vernik, D. E. Kirichenko, V. V. Dotsenko, R. Miller, *et al.*, “Cryocooled wideband digital channelizing radio-frequency receiver based on low-pass ADC”, *Superconductor Science and Technology*, vol.20, no.11, pp.S323–S327, doi:10.1088/0953-2048/20/11/s05, 2007.
  - [36] D. Gupta, D. E. Kirichenko, V. V. Dotsenko, R. Miller, *et al.*, “Modular, multi-function digital-rf receiver systems”, *IEEE Transactions on Applied Superconductivity*, vol.21, no.3, pp.883–890, doi:10.1109/tasc.2010.2095399, 2011.
  - [37] S. Sarwana, D. E. Kirichenko, V. V. Dotsenko, A. F. Kirichenko, *et al.*, “Multi-band digital-rf receiver”, *IEEE Transactions on Applied Superconductivity*, vol.21, no.3, pp.677–680, doi:10.1109/tasc.2010.2098012, 2011.
  - [38] “SEEQC: Chip foundry”, Available at: <https://seeqc.com/chip-foundry-services>, .
  - [39] B. J. Taylor, S. A. E. Berggren, M. C. O’Brien, M. C. deAndrade, *et al.*, “Characterization of large two-dimensional YBa<sub>2</sub>Cu<sub>3</sub>O<sub>7-δ</sub> SQUID arrays”, *Superconductor Science and Technology*, vol.29, no.8, article no.084003, doi:10.1088/0953-2048/29/8/084003, 2016.
  - [40] E. Y. Cho, M. K. Ma, C. Huynh, K. Pratt, *et al.*, “YBa<sub>2</sub>Cu<sub>3</sub>O<sub>7-δ</sub> superconducting quantum interference devices with metallic to insulating barriers written with a focused helium ion beam”, *Applied Physics Letters*, vol.106, no.25, article no.252601, doi:10.1063/1.4922640, 2015.
  - [41] Z. Chen, Y. Li, R. Zhu, J. Xu, *et al.*, “High-temperature superconducting YBa<sub>2</sub>Cu<sub>3</sub>O<sub>7-δ</sub> josephson junction fabricated with a focused helium ion beam”, *Chinese Physics Letters*, vol.39, no.7, article no.077402, ISSN 1741-3540, doi:10.1088/0256-307x/39/7/077402, 2022.
  - [42] S. Ouanani, J. Kermorvant, C. Ulysse, M. Malnou, *et al.*, “High-T<sub>c</sub> superconducting quantum interference filters (SQIFs) made by ion irradiation”, *Superconductor Science and Technology*, vol.29, no.9, article no.094002, doi:10.1088/0953-2048/29/9/094002, 2016.
  - [43] E. R. Pawlowski, J. Kermorvant, D. Crété, Y. Lemaître, *et al.*, “Static and radio frequency magnetic response of high T<sub>c</sub> superconducting quantum interference filters made by ion irradiation”, *Superconductor Science and Technology*, vol.31, no.9, article no.095005, doi:10.1088/1361-6668/aad275, 2018.
  - [44] F. Couëdo, E. R. Pawlowski, J. Kermorvant, J. Trastoy, *et al.*, “High-T<sub>c</sub> superconducting detector for highly-sensitive microwave magnetometry”, *Applied Physics Letters*, vol.114, no.19, article no.192602, doi:10.1063/1.5090175, 2019.
  - [45] B. Müller, M. Karrer, F. Limberger, M. Becker, *et al.*, “Josephson junctions and squids created by focused helium-ion-beam irradiation of YBa<sub>2</sub>Cu<sub>3</sub>O<sub>7-δ</sub>”, *Physical Review Applied*, vol.11, no.4, article no.044082, doi:10.1103/physrevapplied.11.044082, 2019.
  - [46] P.-Y. Xiong, F.-C. Chen, Z.-P. Feng, J.-T. Yang, *et al.*, “Optimization of large-area YBa<sub>2</sub>Cu<sub>3</sub>O<sub>7-δ</sub> thin films by pulsed laser deposition for planar microwave devices”, *Chinese Physics B*, vol.32, no.7, article no.077402, doi:10.1088/1674-1056/acb4d, 2023.
  - [47] I. I. Soloviev, V. I. Ruzhickiy, N. V. Klenov, S. V. Bakurskiy, and M. Y. Kupriyanov, “A linear magnetic flux-to-voltage transfer function of a differential DC SQUID”, *Superconductor Science and Technology*, vol.32, no.7, article no.074005, doi:10.1088/1361-6668/ab0d73, 2019.
  - [48] S. V. Polonsky, V. K. Semenov, and P. N. Shevchenko, “PSCAN: Personal superconductor circuit analyser”, *Superconductor Science and Technology*, vol.4, no.11, pp.667–670, doi:10.1088/0953-2048/4/11/031, 1991.
  - [49] S. Polonsky, P. Shevchenko, A. Kirichenko, D. Zinoviev, and A. Ryljakov, “PSCAN’96: New software for simulation and optimization of complex RSFQ circuits”, *IEEE Transactions on Applied Superconductivity*, vol.7, no.2, pp.2685–2689, doi:10.1109/77.621792, 1997.